Arch. Metall. Mater. **66** (2021), 4, 971-975

DOI: 10.24425/amm.2021.136408

JIN MAN JANG[1,2], WONSIK LEE[1*], SE-HYUN KO[1]

THE EFFECTS OF GRAIN BOUNDARY STRUCTURES ON MECHANICAL PROPERTIES IN NANOCRYSTALLINE Al ALLOY

This study investigates the effects of grain boundary structures on mechanical properties of nanocrystalline Al-0.7Mg-1.0Cu alloy using nanoindentation system. Grain boundary structure transforms to high angle grain boundaries from low angle ones with increase of heat treatment temperature and the transformation temperature is about 400°C. Young's modulus and hardness are higher in sample with low angle grain boundaries, while creep length is larger in sample with high angle ones. These results indicate that progress of plastic deformation at room temperature is more difficult in sample with low angle ones. During compression test at 200°C, strain softening occurs in all samples. However, yield strength in sample with low angle grain boundaries is higher twice than that with high angle ones due to higher activation energy for grain boundary sliding.

Keywords: nanocrystalline Al alloy, Young's modulus, hardness, nanoindentation, low and high angle grain boundary

1. Introduction

Nanocrystalline materials are of great interest since it is known that they have some attractive properties such as high yield strength, improved wear resistance, and superplasticity, and softening at relatively low temperatures compared to the coarse grained materials [1-3].

In nanocrystalline materials, the dislocation mechanism that governs the plasticity of the bulk is no longer possible [4,5]. It means that the dominant deformation mechanism is not based on dislocation pile-up, but grain boundary processes such as grain boundary sliding [5,6]. Grain boundary sliding is closely related to grain boundary structure. Statistical analysis results of the crystalline orientations in superplastically deformed Al alloy have indicated that the grain boundary structure mainly consists of high angle [7]. This observation is consistent with the basis of grain boundary sliding that most of the grain boundary sliding can happen at high angle grain boundaries and the occurrence of extensive grain boundary sliding will finally lead to a random misorientation angle distribution [8,9].

One particular property which can estimate the degree of grain boundary misorientation is the Young's modulus [10]. Young's modulus can be evaluated by several mechanical tests such as bulge, resonance, nanoindentation, tension and so on. Among these methods, a fairly efficient and convenient method is nanoindentation [11]. Many articles about the analysis of mechanical properties using nanoindentation have been reported [12-16]. However, most of the papers focus on the effect of grain size [12-14], and only recently some papers have published about the effect of grain boundary misorientation on mechanical properties using the simulation method [15,16]. Those papers reported that indentation hardness and Young's modulus are higher in materials with low angle grain boundaries than those with high angle ones. And the cause is that the grain boundary deformation, generated by the dislocation pile-up and propagation induced by the indentation stress, occurs more easily at high angle grain boundaries with higher mobility. Therefore, in this paper, the effects of the grain boundary structure on the mechanical properties of the nanocrystalline Al alloy were experimentally examined using nanoindentation. And also, the effects of the degree of misorientation in the nanocrystalline Al alloy on the deformation behavior by grain boundary sliding were investigated.

2. Experimental

Elemental Al(99.5 wt.%), Mg(99.9 wt.%) and Cu(99.9 wt.%) powders were used for production of Al alloy with nomi-

[1] KOREA INSTITUTE OF INDUSTRIAL TECHNOLOGY, INCHEON, 21999, REPUBLIC OF KOREA
[2] INHA UNIVERSITY, DEPARTMENT OF MATERIALS SCIENCE AND ENGINEERING, INCHEON, 22212, REPUBLIC OF KOREA
* Corresponding author: wonslee@kitech.re.kr

nal composition of Al-0.7 wt.%Mg-1.0 wt.%Cu. The elemental powders were mechanically alloyed using attrition ball mill. The stainless steel canister and balls were used in attrition milling. To avoid contamination, the inner surface of canister and balls were coated with Al. The powders and balls were charged into the canister under Ar atmosphere. A ball-to-powder weight ratio was 75:1 and mechanical alloying was conducted for 4 hrs. with milling speed of 320 rpm. To prevent excessive cold welding of powders, methyl alcohol of 1% by weight of powders was added as the process control agent.

Hot pressing was carried out to fabricate the nanocrystalline bulk Al alloy. The mechanically alloyed powders were packed in a mold and hot pressed at a low temperature of 200°C, to avoid the change of grain boundary structures resulting from grain growth. Then, the samples were heat treated for specific time at different temperatures to investigate the change of grain boundary structures. The heat treatment was conducted in flowing N_2 gas to avoid oxidation.

The hardness, Young's modulus and creep length were measured using nanoindentation system with Berkovich indenter. In nanoindentation tests, applied maximum load, loading rate and holding time were decided to 196 mN, 17.6 mN s^{-1} and 10 s respectively. Nine indentations were made on each sample. The hold step was needed to eliminate the influence of creep on the unloading characteristics. Compression test was performed at 200°C with an initial strain rate of 1×10^{-3} s^{-1}.

The densities of the samples were measured using the Archimedes' method. The microstructures and grain sizes were examined using TEM & Digital micrograph (DM) software script.

3. Results and discussion

The chemical composition of the sample hot pressed was measured by ICP and the result is shown in Table 1. The analyzed composition was similar to nominal one. However, Fe content of 0.32 wt.% was detected, which would be mainly contaminated from canister and balls.

TABLE 1

Nominal and analyzed compositions of Al alloy used in this work

Composition (wt.%)	Al	Mg	Cu	Fe
Nominal	Bal.	0.7	1.0	—
Analytical	Bal.	0.75	0.93	0.32

3.1. Microstructure after heat treatment

The fact that many nano sized grains within mechanically alloyed powders have low angle grain boundaries is empirically accepted in our laboratory. Thus, in this work, hot pressing was carried out at 200°C, relatively very low temperature, to sustain still low angle grain boundaries and followed by heat treatment at some different temperatures, expecting that grain boundary structure is changed with heat treatment temperature, i.e., from low angle boundaries to high angle ones. Nanoindentation tests were performed after heat treatment to investigate the effects of grain boundary structures on mechanical properties such as hardness and Young's modulus. In nanocrystalline materials, the hardness changes with grain size according to the Hall-patch equation [17] or inverse Hall-Patch equation [18], and Young's modulus decreases due to the increase in the interaction distance between atoms in grain boundaries as grain size decreases [19,20]. Therefore, to observe the effect of the difference in grain boundary structure, excluding the effect of grain size, all samples must have the same grain size. For this reason, heat treatment time was decided at each temperature by grain growth equation as follows:

$$D^n - D_0^n = Kt \tag{1}$$

where D and D_0 are grain sizes after and before heat treatment, t is heat treatment time, n and K are constants. The constant K in Eq. (1) depends on temperature and can be described by an arrhenius type equation,

$$K = K_0 \exp(-Q/RT) \tag{2}$$

where Q is apparent activation energy for grain growth and K_0 is a constant. The values of n and Q were obtained as 2 and 50.4 kJ/mole·K^{-1} respectively, calculated using grain growth curves in a previous report [21] which were gotten in Al alloys similar to that in this work. Table 2 shows heat treatment times calculated from the above values at different temperatures and relative densities of the samples after heat treatment.

TABLE 2

Heat treatment conditions in this work and relative densities of samples heat treated in the conditions

Heat treatment conditions		Relative density (%)
Temperature (°C)	Time (min)	
250	895	92.4
300	320	92.6
350	136	93.1
400	65	91.3
500	20	91.6

TEM observation was performed to examine microstructures of the samples heat treated. All the samples heat treated had average grain sizes of 50 to 60 nm, indicating that the purpose to obtain the same grain size was successfully achieved, though grain size was larger a little at higher temperature. Fig. 1 shows TEM micrographs of samples heat treated at 250°C and 400°C, respectively. From bright and dark field images, it can be seen that average grain sizes are about 50 nm and 60 nm in both samples respectively. In selected area diffraction (SAD) pattern of Fig. 1(a), some diffraction spots are concentrated on specific positions. This means that the microstructure of the sample heat treated at 250°C is still composed of many low angle grain boundaries, measured about 10 degrees or less, although some

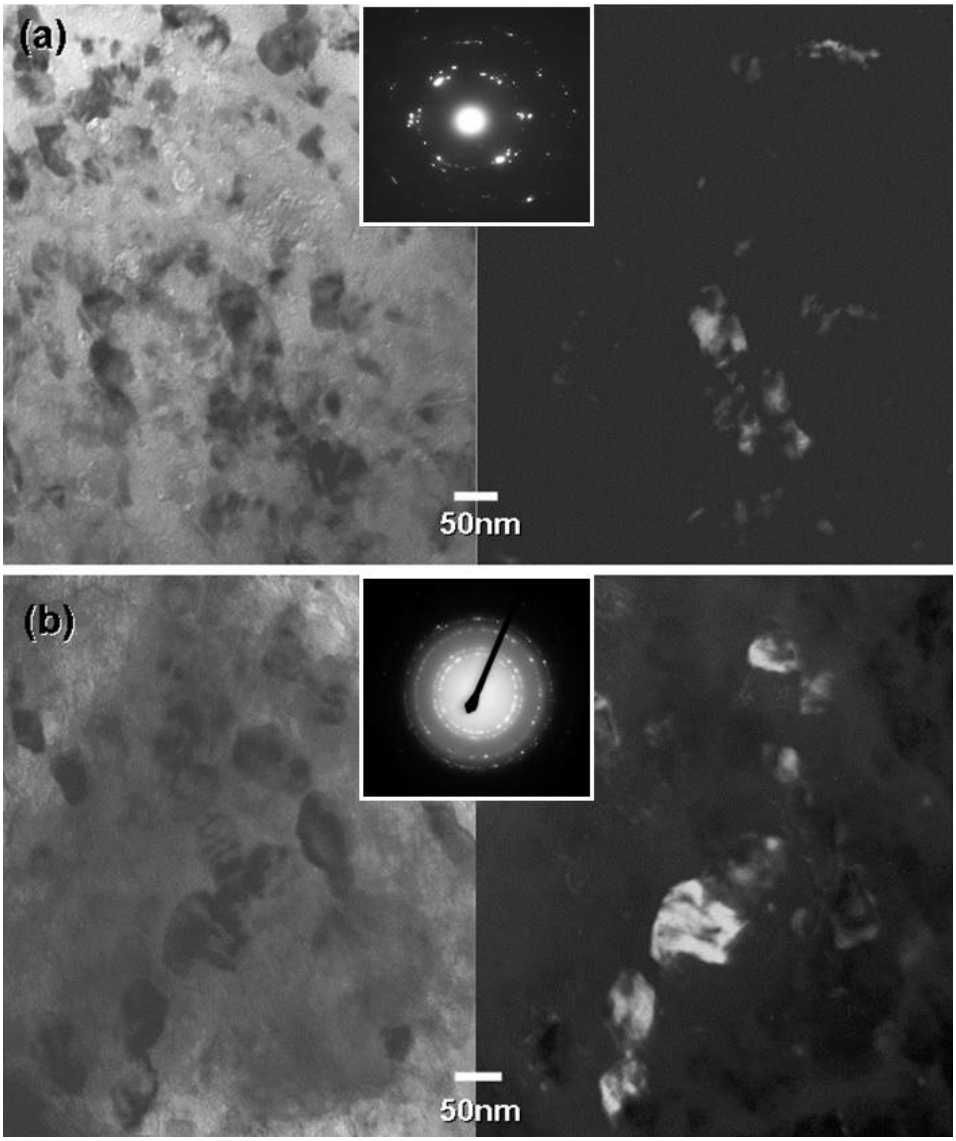

Fig. 1. TEM micrographs of samples heat treated at (a) 250°C and (b) 400°C, respectively

spots by high angle boundaries were partially distributed. On the other hand, clear rings are shown in SAD pattern obtained in the sample heat treated at 400°C (Fig. 1(b)), which means that grain boundaries in this sample are almost high angle. The results of TEM observation strongly indicate that the grain boundary structure is transformed from a low angle grain boundary into a high angle grain boundary. It is considered that this is based on the Cahn-Cottrell model in which grain growth occurs with increasing temperature after the formation of nuclei having high-angle grain boundaries, generated by the migration of low angle grain boundaries during the recovery process [22-24].

3.2. Nanoindentation

Some representative load-penetration depth curves obtained in nanoindentation test are shown in Fig. 2. Difference in penetration depth (h_{max}) and contact stiffness (S) appears distinctly in the samples tested, which is due to change of grain boundary structure by heat treatment. From these curves, the hardness, Young's modulus and creep length were calculated by Oliver and Pharr data analysis method [25]. Fig. 3 shows the variations of Young's modulus, hardness and creep length with heat treatment temperature. Young's modulus, hardness and creep length in sample heat treated at 250°C were similar to those in as-hot pressed sample. But at above 250°C, Young's modulus and hardness tend to decrease while creep length increase with increase of temperature (tendency that Young's modulus increases again and creep length decreases at above 400°C might result from some increase in grain size). Considering the results of TEM observation in Fig. 1, these trends of the mechanical properties obviously result from the difference of grain boundary structures, i.e., low and high angle boundaries, and consequently, it is suggested that Young's modulus is higher in materials with low angle grain boundaries and progress of plastic deformation at room temperature is easier in nanocrystalline materials with high angle grain boundaries. The transformation temperature from low angle grain boundary into high angle one is evaluated about 400°C in this work.

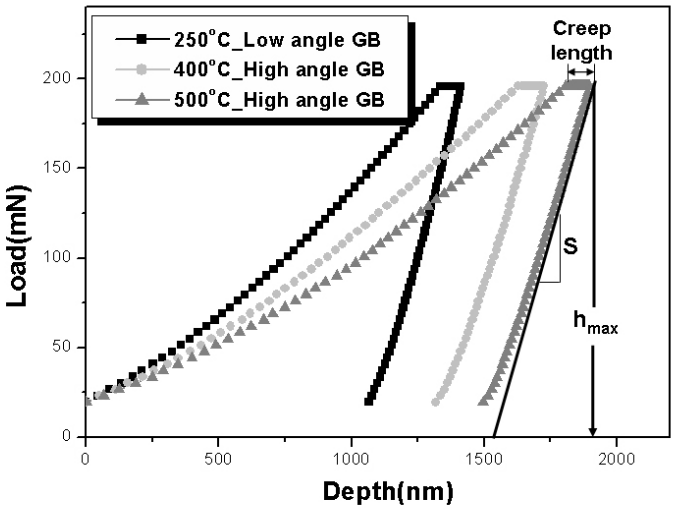

Fig. 2. Some representative load-penetration depth curves obtained in nanoindentation test

Hardness and Young's modulus are also affected by porosity, especially in sintered materials like samples used in this work. However, the porosity effect can be eliminated when indentation size is sufficiently smaller than particle size [26]. Indentation sizes in all samples were ranged about from 5 μm to 20 μm while particle sizes after heat treatment observed by SEM were more than 100 μm, and relative densities were almost the same as can be seen in Table 2. Consequently, porosity effect can be ignored in this study.

3.3. Compression test

To investigate the effect of the low and high angle grain boundary structures on deformation behavior, compressive tests were carried out at 200°C. Fig. 4 shows compressive true stress-true strain curves of samples heat treated at 250°C and 400°C

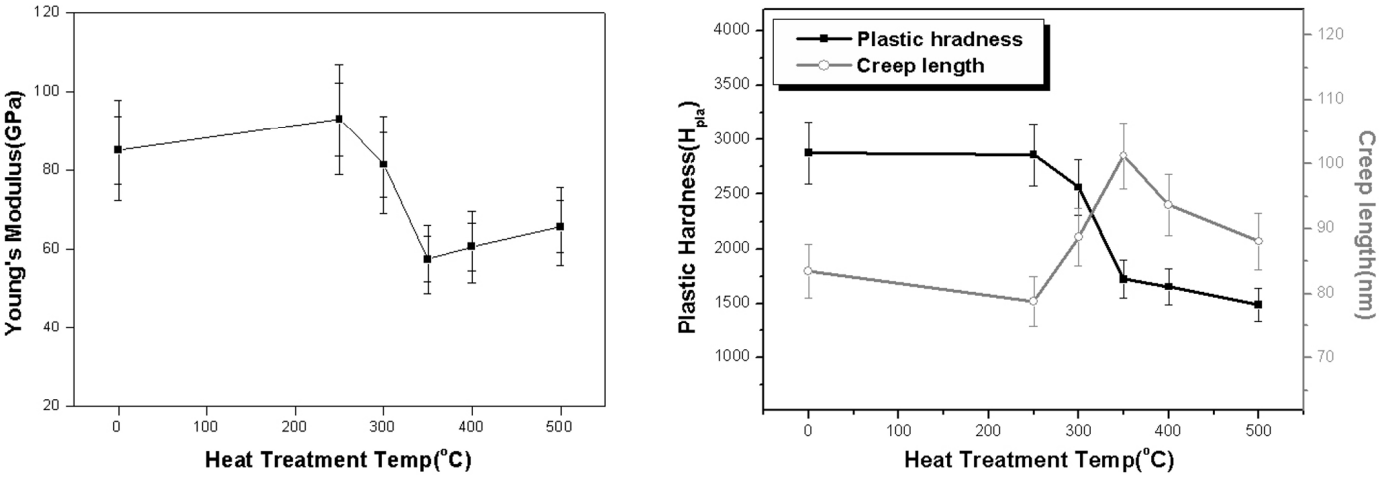

Fig. 3. Variations of Young's modulus, hardness and creep length with heat treatment temperature

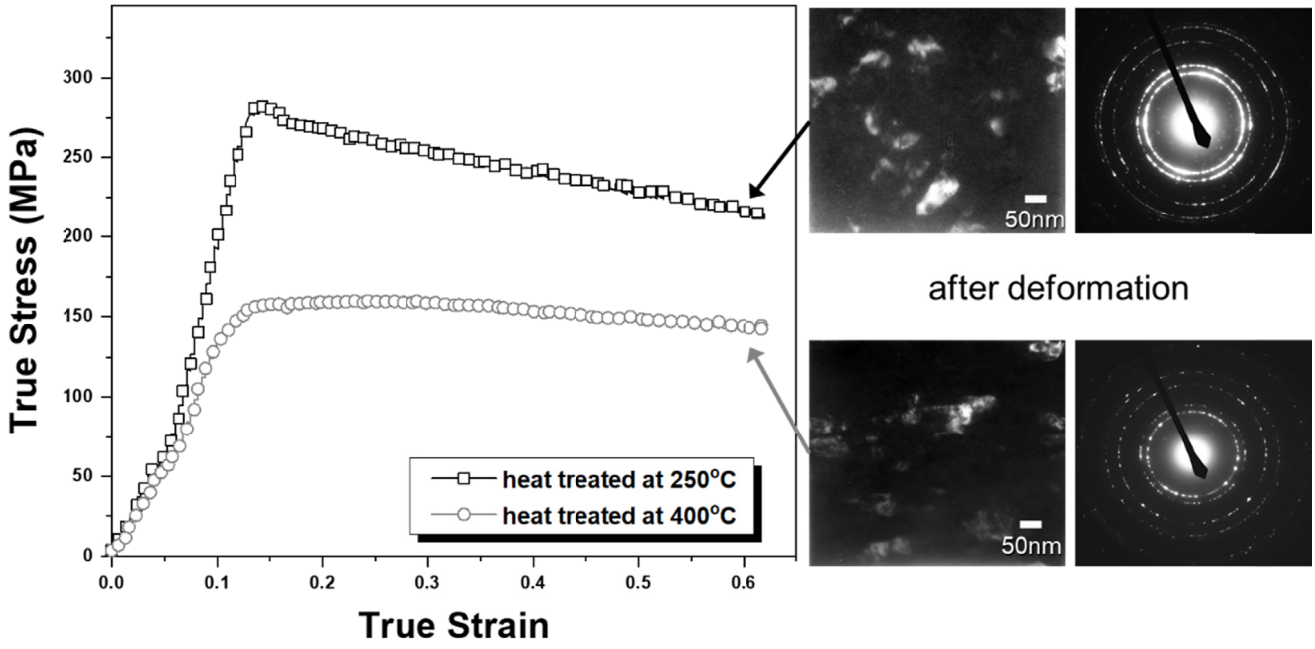

Fig. 4. Compressive true stress-true strain curves of samples with low and high angle grain boundaries (initial strain rate of 1×10^{-3} s^{-1})

respectively. As already mentioned above, both samples are composed of low and high angle grain boundaries, respectively. As shown in Fig. 4, strain softening phenomenon occurred in all of both samples. Also, yield strength of sample with low angle grain boundaries was higher twice than that with high angle grain boundaries, which means that activation energy for grain boundary sliding is higher in sample with low angle grain boundaries.

Microstructural change after compression test was investigated by TEM. After compressive test at 200ºC, the average grain sizes were measured about 100 nm in both samples. SAD patterns showed clear rings due to high angle grain boundaries in all the samples, indicating that low angle grain boundaries were transformed into high angle boundaries during deformation. This result is well consistent with the basis of grain boundary sliding – the occurrence of extensive grain boundary sliding will finally lead to a random misorientation angle distribution [8,9].

4. Conclusions

The effects of grain boundary structures on mechanical properties were investigated in nanocrystalline Al-0.7 wt.%Mg-1.0 wt.%Cu alloy.

1. Grain boundary structure was transformed low angle grain boundary into high angle one with increase of heat treatment temperature and the transformation temperature was measured about 400ºC.
2. Young's modulus and hardness were higher in sample with low angle grain boundaries, which indicate that progress of plastic deformation at room temperature is easier in nanocrystalline materials with high angle grain boundaries.
3. Yield strength in sample with low angle grain boundaries was higher twice than the one with high angle grain boundaries, which is originated from higher activation energy for grain boundary sliding of low angle grain boundaries.

Acknowledgments

This study has been conducted with the support of the Korea Institute of Industrial Technology as "Development of root technology for multi-product flexible production (kitech EO-20-0015)"

REFERENCES

[1] J. Cintas, E.S. Caballero, J.M. Montes, F.G. Cuevas, C. Arevalo, Adv. Mater. Sci. Eng. **2014**, 1 (2014).
[2] Y. Liu, Z. Han, H. Cong, Wear **268**, 976 (2010).
[3] G. Jeong, J. Park, S. Nam, S.E. Shin, J. Shin, D. Bae, H. Choi, Archives of Metallurgy and Materials **60** (2), 1287 (2015).
[4] M. Yu. Gutkin, I.A. Ovid'ko, N.V. Skiba, Phys. Solid State **47**, 1662 (2005).
[5] H. Van Swygenhoven, M. Spaczer, A. Caro, Acta Mater. **47**, 3117 (1999).
[6] Y. Xun, M.J. Tan, K.M. Liew, Scripta Mater. **61** (1), 76 (2009).
[7] Y. Xun, M.J. Tan, K.M. Liew, J. Mater. Processing Tech. **162-163**, 429 (2005).
[8] T.J. Rupert, J. Appl. Phys. **114**, 033527 (2013).
[9] T.R. McNelly, D.L. Swisher, M.T. Perez-Prado, Metall. Mater. Trans. **A 33**, 279 (2002).
[10] Y. Rao, A.J. Waddon, R.J. Farris, Polymer **42** (13), 5925 (2001).
[11] A.C. Fisher-Crips, Nanoindentation, Springer-Verlag, New York 2002.
[12] M.S. Asl, B. Nayebi, A. Motallebzadeh, M. Shokouhimehr, Compos. B Eng. **175**, 107153 (2019).
[13] S. Sinha, R. Mirshams, T. Wang, S. Nene, M. Frank, K. Liu, R. Mishra, Sci. Rep. **9**, 6639 (2019).
[14] L. Melk, J.J.R. Rovira, F. García-Marro, M.-L. Antti, B. Milsom, M.J. Reece, M. Anglada Ceram. Int. **41**, 2453 (2015).
[15] G. He, C. Xu, C. Liu, H. Liu, Mater. Des. **202**, 109459 (2021).
[16] Q. Duan, H. Pan, B. Fu, J. Yan, Steel Res. Int. 2019, 1900317 (2019).
[17] C.S. Pande, K.P. Cooper, Prog. Mater. Sci. **54** (6), 689 (2009).
[18] C. Zheng, Y.W. Zhang, Mater. Sci. Eng. A **423** (1-2), 97 (2006).
[19] C.-W. Nan, X. Li, K. Cai, J. Tong, J. Mater. Sci. Letters **17** (22), 1917 (1998).
[20] M. Becton, X. Wang, Phys. Chem. Chem. Phys. **17**, 21894 (2015).
[21] H. Hasegawa, S. Komura, A. Utsunomiya, Z. Horita, M. Furukawa, M. Nemoto, T.G. Langdon, Mater. Sci. Eng. A **265**, 188 (1999).
[22] P.R. Rios, F.S. Jr, H.R.Z. Sandim, R.L. Plaut, A.F. Padiha, Mater. Research **8** (3), 225 (2005).
[23] AH. Cottrell In: Chalmers B, editor. Theory of dislocations, Progress in Metal Physics. **4**, 251 (1953) London, Pergamon Press.
[24] R.W. Cahn, Proceedings of the Physical Society, Ser. AI. **63** (364), 323 (1950).
[25] W.C. Oliver, G.M. Pharr, J. Mater. Res. **7**, 1564 (1992).
[26] D. Jang, M. Atzmon, J. App. Phy. **93** (11), 9282 (2003).